Zoomorphology (2014) 133:111–126
DOI 10.1007/s00435-013-0207-2

ORIGINAL PAPER

Variation in setal micromechanics and performance of two gecko species

Travis J. Hagey · Jonathan B. Puthoff · Madisen Holbrook · Luke J. Harmon · Kellar Autumn

Received: 5 April 2013 / Revised: 30 September 2013 / Accepted: 7 October 2013 / Published online: 20 November 2013
© Springer-Verlag Berlin Heidelberg 2013

Abstract Biomechanical models of the gecko adhesive system typically focus on setal mechanics from a single gecko species, *Gekko gecko*. In this study, we compared the predictions from three mathematical models with experimental observations considering an additional gecko species *Phelsuma grandis*, to quantify interspecific variation in setal micromechanics. We also considered the accuracy of our three focal models: the frictional adhesion model, work of detachment model, and the effective modulus model. Lastly, we report a novel approach to quantify the angle of toe detachment using the Weibull distribution. Our results suggested the coupling of frictional and adhesive forces in isolated setal arrays, first observed in *G. gecko* is also present in *P. grandis* although *P. grandis* displayed a higher toe detachment angle, suggesting they produce more adhesion relative to friction than *G. gecko*. We also found the angle of toe detachment accurately predicts a species' maximum performance limit when fit to a Weibull distribution. When considering the energy stored during setal attachment, we observed less work to remove *P. grandis* arrays when compared with *G. gecko*, suggesting *P. grandis* arrays may store less energy during attachment, a conclusion supported by our model estimates of stored elastic energy. Our predictions of the effective elastic modulus model suggested *P. grandis* arrays to have a lower modulus, E_{eff}, but our experimental assays did not show differences in moduli between the species. The considered mathematical models successfully estimated most of our experimentally measured performance values, validating our three focal models as template models of gecko adhesion (see Full and Koditschek in J Exp Biol 202(23):3325–3332, 1999), and suggesting common setal mechanics for our focal species and possibly for all fibular adhesives. Future anchored models, built upon the above templates, may more accurately predict performance by incorporating additional parameters, such as variation in setal length and diameter. Variation in adhesive performance may affect gecko locomotion and as a result, future ecological observations will help to determine how species with different performance capabilities use their habitat.

Keywords Frictional adhesion · Work of detachment · Effective elastic modulus · Weibull distribution · Toe detachment angle · Template model

Communicated by A. Schmidt-Rhaesa.

Data Accessibility: R scripts and raw data available from the Dryad Digital Repository: http://doi.org/10.5061/dryad.cr1c1.

T. J. Hagey (✉) · L. J. Harmon
Department of Biological Sciences, University of Idaho, Moscow, ID, USA
e-mail: tjhagey@uidaho.edu

J. B. Puthoff · M. Holbrook · K. Autumn (✉)
Biology Department, Lewis & Clark College, Portland, OR, USA
e-mail: autumn@lclark.edu

Introduction

Geckos are well known for their climbing abilities. The gecko adhesive system uses arrays of setae, which are hairlike keratinized epidermal derivatives on the underside of each toe (Alibardi et al. 2007; Federle 2006; Maderson 1964; Peattie 2009; Ruibal and Ernst 1965; Russell 2002). Each seta is branched into hundreds of terminal ends called spatulae that interact with a substrate via van der Waals interactions (Autumn et al. 2000, 2002; Puthoff et al. 2010). Though these substrate/seta interactions are

individually minute, the net attraction can be considerable given the multiplicity of these structures (Autumn et al. 2000). As a result, geckos' specialized toe pads are capable of generating large frictional and adhesive forces (Autumn et al. 2000; Irschick et al. 1996).

The performance of the gecko adhesive system is influenced strongly by the morphology of setae, the toe, and foot (Gamble et al. 2012; Peattie 2007; Russell 2002), which together creates the sum of the hierarchical gecko adhesive system. Despite the biomechanical complexity of the system, relatively simple models have been developed describing particular performance aspects of isolated setal arrays (Autumn et al. 2006a, 2006b; Gravish et al. 2008; Hansen and Autumn 2005; Pesika et al. 2009; Pugno and Lepore 2008a; Tian et al. 2006). In this study, we focused on predicted and observed performance at the setal array level. Most setal biomechanical models were derived using data from only a single species, *Gekko gecko.* Among gecko species, there is considerable diversity in setal morphological characteristics such as length, width, packing density, and branching pattern within and between species (Bauer 1998; Johnson and Russell 2009; Peattie 2007; Ruibal and Ernst 1965; Williams and Peterson 1982). We propose that small differences in setal morphology will directly influence the performance of setal arrays. We investigated similarities and differences in setal morphology and performance between the previously considered species *G. gecko* and the distantly related gecko species *Phelsuma grandis* (Gamble et al. 2012; Pyron et al. 2013). We chose these two species for our study because of their phylogenetic distance and superficially similar setal morphology and organization. Both species exhibit setal curvature and have setae that are angled at rest, suggesting common setal mechanics. Both species are also arboreal and found in humid tropical environments (Glaw and Vences 2007; Rosler et al. 2011). The mathematical models we considered here were described using observations from *G. gecko*, and we expect our observations from this species to be similar to previously published results, serving as a positive control as well as illustrating the potential variation inherent in observations of the gecko adhesive system.

We compared observed and expected setal performance values using three previously described models with the goal of highlighting strengths and weaknesses of these models when applied beyond *G. gecko* (Autumn et al. 2006a, 2006b; Gravish et al. 2008). Our model estimations and experimental measurements predominately considered two types of forces: negative forces normal to the plane of contact, termed adhesive forces, and frictional forces, which are parallel to the contact surface. The frictional adhesion (FA) model describes the interplay between frictional and adhesive forces generated by a setal array (Autumn et al. 2006a; Fig. 1a). The work of detachment (WoD) model describes changes in stored elastic energy and frictional losses during setal removal from a substrate (Gravish et al. 2008; Fig. 1b). Lastly, the effective modulus model (EM) considers the homogenized compressive deformation properties of a setal array (Autumn et al. 2006b; Fig. 1c). These three models provide a quantitative basis for comparing the performance of our focal species by direct experiment and theoretical estimation, with the two latter models using setal morphology as input values. These approaches allowed us to investigate what effect morphological differences will have on adhesive performance. Our proposed hypotheses also have broader ramifications for connections between setal morphology, array performance, and whole-animal locomotion and ecology. We describe the three models of interest in more detail below.

Frictional adhesion (FA) model

"Frictional adhesion" refers to the coupling of frictional and adhesive forces generated by a setal array in contact with a substrate (Autumn et al. 2006a). Figure 1a inset (i) illustrates typically observed adhesion forces (blue) and frictional forces (green) during a steady drag across a substrate. Under the FA model, the adhesion of a gecko toe is related to the strength of the frictional force. If a setal array generates a friction force of $F_{\parallel}$, then the adhesion force $(F_{\perp})$ produced cannot exceed $F_{\parallel}$ tan (α*) as summarized by:

$$F_{\parallel} \geq \frac{F_{\perp}}{\tan \alpha^{*}} \quad (1)$$

where α* is the critical force angle at which setae detach spontaneously from the substrate (Autumn et al. 2006a). Higher α* values allow more adhesion to be generated considering a given amount of friction (Autumn et al. 2006a). The physical basis of the frictional adhesion effect in setal arrays is currently a very active area of research (see Chen et al. 2008, 2009; Tian et al. 2006; Yamaguchi et al. 2009).

Since α* is a property of individual setae and requires laboratory instruments to measure, Autumn et al. (2006a) proposed a whole-animal performance assay as a proxy to measure a species' maximum critical angle. This assay, called TAD (toe angle of detachment, $\bar{\alpha}^{*}$), quantifies the maximum angle of a surface in which a suspended gecko's toe can adhere to using the Weibull distribution (see "Materials and methods" section; Fig. 1a, inset (iii); Fig. 2). This assay is easier to conduct than assays using isolated setal arrays and can even be employed in the field. In addition, this assay is weight independent and likely related to setal morphology (Fig. 2; Autumn et al. 2006a).

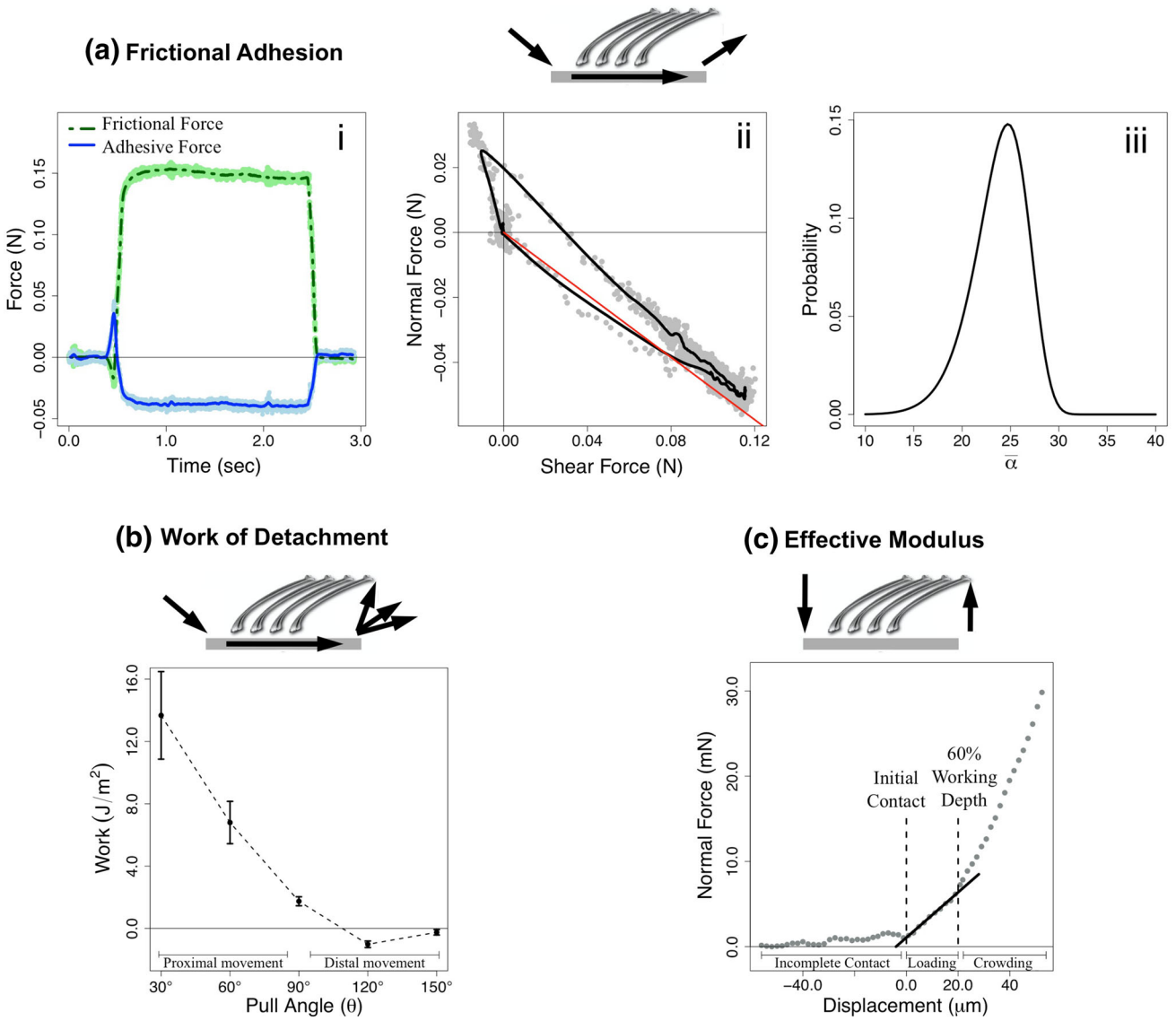

Fig. 1 Our three biomechanical models of interest are the frictional adhesion (FA) model (section **a**, *shown at top*), work of detachment (WoD, section **b**, *lower left*), and effective modulus (EM, section **c**, *lower right*). At the *top* of each compartment, we illustrate the kinematics of the testing procedure. Generalized *graphs*, *highlighting typical measurements* from our assays are also illustrated. In assays regarding the FA model (**a**), we use a load-drag-pull protocol (see "Material and methods" section). Plot *i* illustrates typical frictional and adhesive forces (*green* and *blue*, respectively) produced by an isolated setal array through the course of a singe performance trial measured through time. Plot *ii* displays typically observed frictional and adhesive forces plotted against one another. From these data, we can determine α* (for details see "Material and methods" section and Autumn et al. 2006a). The *red line* represents the maximum force angle typically determined from toe detachment trials with a slope of tan ($\bar{\alpha}^*$). In the third plot, *iii*, we illustrate a Weibull probability distribution ($p[\bar{\alpha}^*]$; $\lambda = 26$, $m = 10$). Note the distribution's tails illustrating how the Weibull distribution are different from the normal distribution. The left tail accounts for early failures as expected by a time-dependent failure process. In section **b**, kinematics of a modified LDP used for our WoD assays can be seen, illustrating multiple pull-off angles. We used pull-off angles (θ) of 30°, 60°, 90°, 120°, and 150° relative to the substrate. Pull-off angles under 90° (movement against the natural curvature of the setae) result in proximal movement of array relative to the original orientation on the animal. Angles over 90° represent movement opposite to the testing drag direction, and distal relative to the array's location on the animal before removal. Observed work typically decreases as pull-off angle approaches 120°. During our EM testing (**c**), we removed the drag section of the LDP procedure, allowing the array to make contact and be removed vertically from the substrate without any lateral movement. Using the observed normal force and vertical displacement values, we can determine the three phases of compression; incomplete contact, elastic compression and setal crowding and estimate effective modulus as the *slope of a line* through the elastic compression stage of loading

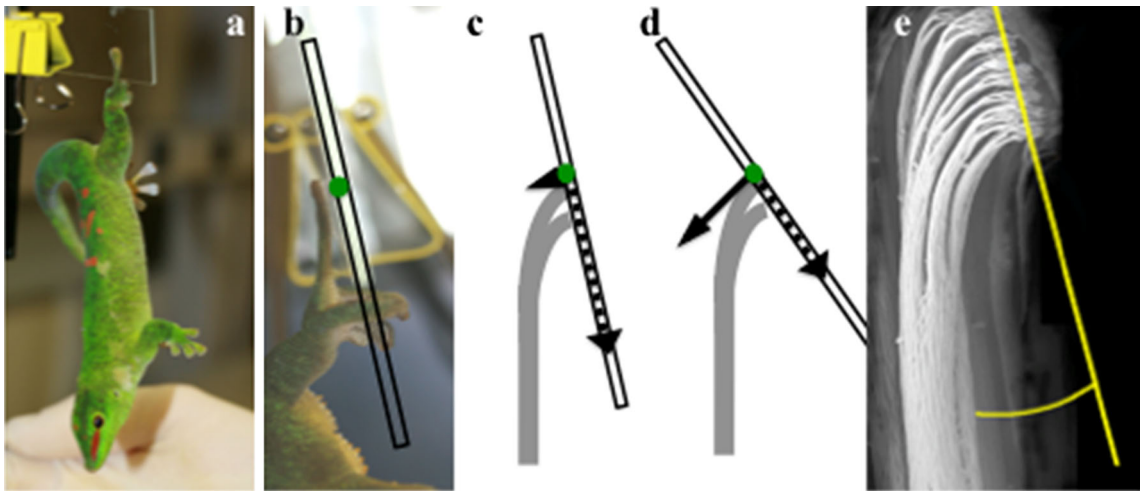

Fig. 2 To measure toe detachment angle (TAD), we suspended a live, non-sedated gecko from a single rear, middle toe from a clean glass microscope slide using the animal's natural clinging ability (**a**, **b**). Force diagrams (**c**, **d**) illustrate an idealized seta interacting with the substrate as it moves from vertical to an inverted orientation. During the assay, the setal shaft angle increases relative to the substrate and the generated forces transition from friction to a combination of friction and adhesion until the toe pad spontaneously detaches. At the angle of toe detachment, the seta is at the force angle limit described by the FA model. Autumn et al. (2006a) hypothesized the angle of spontaneous detachment is related to the setal miter angle (**e**)

Using TAD observations, we can quantify the maximum ratio between adhesion and friction a species can generate, as dictated by the FA model (Fig. 2 and Eq. 1).

We can also use $\bar{\alpha}^*$ to represent the maximum α* value achievable by isolated setal arrays. Both $\bar{\alpha}^*$ and α* can be described as force angles or as force ratios where the tangent of α* or $\bar{\alpha}^*$ is greater than or equal to $\frac{F_\perp}{F_\parallel}$. Figure 1a inset (ii) illustrates typical frictional and adhesive force measurements from isolated setal arrays during a steady drag across a substrate. The adhesion-to-friction ratio upper limit for *G. gecko* (red line) can be observed in quadrant IV. This line has a slope of tan ($\bar{\alpha}^*$) from Autumn et al. (2006a).

We quantified and compared α*, the observed critical angle of setal detachment from setal frictional and adhesive force measurements, and $\bar{\alpha}^*$, a species' toe detachment angle inferred from a collection of toe detachment observations, of our two focal species. We tested whether toe detachment angle $\bar{\alpha}^*$ predicts the maximum force angle α*, as predicted by the FA model. We anticipated that the FA model accurately describes forces generated by *P. grandis* and *G. gecko* setal arrays, although each species may exhibit different performance due to their respective setal morphology.

Work of detachment (WoD) model

When a gecko deploys its adhesive system, the individual adhered setae are placed under tension, changing from a relaxed, curved shape to a straight configuration (Gravish et al. 2008). As a result, energy is stored in the setal array. We can examine how much energy is stored by quantifying the work required to remove the setae from the substrate, shown in Fig. 1b. During detachment, the work required depends on the angle at which the isolated setal array is removed from the substrate, i.e., the pull-off angle (θ), specifically a proximal removal of the array ($\theta < 90°$), a vertical removal ($\theta = 90°$), or a distal removal ($\theta > 90°$). Proximal and distal in this context refer to the original orientation of the array on the animal's toe. During WoD performance assays, θ is an independent variable that is controlled experimentally. With measurements of WoD over a range of pull-off angles, we can generate a WoD vs. pull-off angle data series (Gravish et al. 2008).

Gravish et al. (2008) suggested that frictional sliding of the setal spatulae during detachment at proximal pull-off angles ($\theta < 90°$) contributes the majority of the energy required to detach the array. At pull-off angles near 120°, spatulae sliding is minimal and the release of stored elastic energy dominates the detachment process. The frictional energy loss during detachment due to spatulae slippage ($W_{\parallel\ \mathrm{slip}}$) across detachment angles (θ) and the energy released during detachment at 120° (both lateral and normal components i.e., $W_{\parallel\ \mathrm{elastic}}$ and $W_{\perp\mathrm{elastic}}$) can all be addressed independently. Energy lost due to spatulae slippage ($W_{\parallel\ \mathrm{slip}}$) is given by

$$W_{\parallel\mathrm{slip}}(\theta) = \frac{F_\parallel}{A} s_{\mathrm{slip}} = \frac{F_\parallel}{A}\left[L\left(\cos(\alpha_0) - \cos(\bar{\alpha}*) + \frac{\sin(\bar{\alpha}*) - \sin(\alpha_0)}{\tan\theta}\right)\right], \quad (2)$$

where $F_\parallel/A$ is frictional stress, s_{slip} is the distance the setal tip slides along the substrate, L is the setal length, $\bar{\alpha}^*$ is the maximum critical force angle (the same parameter estimated in the FA model), and α_0 is the angle the seta makes

with the substrate when under drag tension. α_0 can be estimated as $\alpha_0 = \sin^{-1}\left(\frac{H-d}{L}\right)$, where H is the undisturbed array height and d is the working depth (Gravish et al. 2008; see "Materials and methods" section). Note that the variables L, H, and d are inferred from setal measurements where as θ is controlled experimentally.

Pull-off angles of $\theta \approx 120°$ allow very little spatulae slippage (Gravish et al. 2008). Near this pull angle, elastic energy is returned from the relaxing setae ($W_{\parallel\ \text{elastic}}$ plus $W_{\perp\text{elastic}}$). The spring constant (k) for this configuration change is estimated as (Gravish et al. 2008; Persson 2003):

$$k = C\frac{ER^4}{L^3} \tag{3}$$

where C is a geometrical factor of ten according to Persson (2003), E is the Young's modulus of β-keratin, and R is setal radius. It is notable that elastic return is highly dependent on setal curvature; only curved setae can readily store and release elastic energy. Using Eq. (3), we can estimate the lateral elastic energy return during detachment as

$$W_{||\text{elastic}} = \frac{1}{2}\rho k x^2, \tag{4}$$

where ρ is setal density, k is the setal spring constant, and x is the lateral setal displacement during energy storage (Gravish et al. 2008). Energy storage in the normal direction ($W_{\perp\text{elastic}}$) can be estimated as:

$$W_{\perp\text{elastic}} = \frac{E_{eff}(\Delta H)^2}{2H}, \tag{5}$$

where E_{eff} is the effective elastic modulus of a setal array (described below), ΔH is the change in array height, and H is the undisturbed array height (Gravish et al. 2008). The work required to detach arrays and the energy stored during attachment can be modeled with the above equations, using morphology and other values as inputs. In this study, we use the above equations and experimental observations to compare the energy stored during setal attachment of our two focal species.

Effective modulus (EM) model

A gecko's climbing ability depends on how closely its toe pads and setae can conform to the topography of a terrain (Peattie 2009; Russell and Johnson 2007). The ability to establish intimate contact is typically a characteristic only of soft easily deformed materials. Gecko setae are made of β-keratin, a material that is quite stiff in bulk and theoretically unsuitable for adhesion (Autumn et al. 2006b). Nevertheless, setal arrays exhibit considerable sticking force on a wide variety of terrain. This is because, though the individual elements of the array are stiff, the array is, overall, considerably compliant. An intrinsic property of a gecko setal array, called the homogenized or "effective" modulus (E_{eff}), describes the overall stiffness of a setal array. This value can be determined experimentally, similar to a tensile compression test performed on a bulk material specimen. It is important to note that there are secondary effects related to setal crowding during compression (Fig. 1c; Pesika et al. 2009), so care must be taken to isolate the correct deformation regime during analyses. The effective modulus can also be estimated from measurements of setal morphology. The compression properties of the array depend on the bending behavior of the individual seta, which can be described by traditional materials mechanics. Autumn et al. (2006b) determined that

$$E_{eff} = \frac{3EI\rho\ \sin\phi}{L^2\cos^2\phi}, \tag{6}$$

where E is the Young's modulus of β-keratin, L is setal length, I is the second moment of area for the setae (for a cylinder $I = \pi R^4/4$ with R as the radius), ρ is the setal density, and ϕ is the setal resting angle. In this study, we considered E_{eff} experimentally by compressing setal arrays of both focal species and simultaneously recording the force required to do so (see "Materials and methods" section). We also used setal measurements to estimate the expected E_{eff}.

Hypotheses

Our three models make predictions about setal performance. The WoD and EM models describe mechanical relationships between setal morphology and expected performance. The FA model connects setal critical angle, α*, to the ratio of friction and adhesion generated, without a direct relation to setal morphology (but see Chen et al. 2008, 2009; Tian et al. 2006; Yamaguchi et al. 2009). These models were developed considering a single species, *G. gecko*, and in this study, we hypothesize that they will also accurately predict *P. grandis* performance.

Hypothesis 1 (frictional adhesion): The relative ratio of friction to adhesion generated by isolated setal arrays will be limited by a constant force angle (α*, Eq. 1) that we can estimate from the angle of toe detachment ($\bar{\alpha}^*$) for both *G. gecko* and *P. grandis*.

Hypothesis 2 (work of detachment): Using setal morphology as inputs, the WoD model will predict observed work of detachment as a function of pull-off angle ($W_{\parallel\ \text{slip}}$, Eq. 2) and stored energy when spatulae slippage is not present ($W_{\perp elastic}$ Eqs. 3, 4; and $W_{\parallel\ \text{elastic}}$ Eq. 5) for both *G. gecko* and *P. grandis*.

Hypothesis 3 (effective modulus): Using setal geometry as inputs, the EM model (Eq. 6) will predict the observed effective modulus of (E_{eff}) isolated setal arrays for both *G. gecko* and *P. grandis*.

Materials and methods

Setal array collection and substrate preparation

Glass and polytetrafluoroethylene-coated (also known as PTFE or Teflon) microscope slides (Erie Scientific, Portsmouth, NH, USA) were used to remove arrays and as test substrates. Slides were cleaned prior to use with a 15 min 2 M NaOH bath, followed by a triple rinse using deionized water, dried with Kim Wipes (Kimberly-Clark, Neenah, WI, USA) after every rinse, and set aside for up to 24 h.

We harvested intact setal arrays from our two focal species (*G. gecko* and *P. grandis*) by pulling each animal's toe proximally across a clean glass microscope slide, causing a small area of the outer skin layer containing setae to separate from the inner layers (Autumn et al. 2006a). This operation can be performed on non-anesthetized animals with no lasting effects. Setae are regrown and adhesive function recovered after the next molt (Autumn et al. 2006a). When handling our live species, thin strips of adhesive tape were wrapped around the snout of aggressive individuals, with attention to not cover the eyes or nostrils, to prevent bites from occurring (following Autumn et al. 2006a). We mounted our collected setal arrays on aluminum scanning electron microscope (SEM) stubs using cyanoacrylate glue (Loctite 410). Handled delicately, these specimens can perform at full capability through many tests (Autumn et al. 2006b). Arrays were collected using the above technique for both setal morphological measurements and performance assays.

Setal morphology measurements

To measure setal morphology, we collected arrays from one *P. grandis* (seven arrays) and two *G. gecko* lizards (nine arrays total, five or four arrays from each individual). Scanning electron microscope images were collected using an FEI Phenom microscope (Hillsboro, OR, USA). A variable tilt mount provided a wide range of viewpoint options during imaging. Best results were obtained when the array was viewed from the side, with the line of sight perpendicular to the shaft of the setae (see Fig. 4).

Image analysis was performed with ImageJ analysis software (Version 1.44, National Institutes of Health). Using the scale bar imbedded within microscope images, we measured setal length (L; using a four segment line along the setal shaft), setal radius (R; at locations mid-shaft, prior to branching and the setae's distal curvature), resting angle (ϕ), and array height (H). An illustration of these measurements can be seen in Fig. 3. Setal array morphology has been reported to vary within and between scansors in the *Rhoptropus* genus (Johnson and Russell 2009). To reduce intraspecific variation, we limited our morphological measurements to setae in the middle of the removed array; in other words, we did not measure setae that were distally or proximately located on the removed scansor, although we did not control for variation between scansors, and this intraspecific variation may have influenced our measurements.

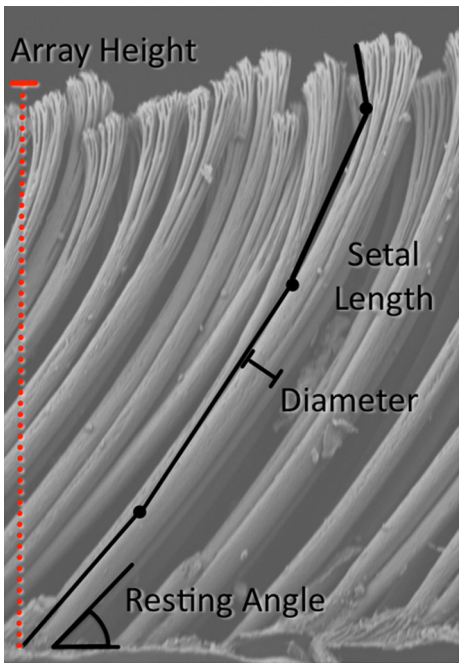

Fig. 3 Our setal morphological measurements were gathered from scanning electron images. We measured four metrics using the integrated image *scale bars*. Setal resting angle was the angle between the base of the setal shaft and the basal skin layer (*lower left*). Setal shaft diameter was measured mid-shaft below the onset of setal branching, setal shaft length was calculated as the summed length of a four segment line, and array height was measured as the overall mean height of the setal array (*red dotted line*)

Frictional adhesion measurements

To determine α*, we measured frictional and adhesive forces generated by isolated setal arrays during a steady drag across a glass substrate using a custom mechanical testing platform called "RoboToe" and employed analysis techniques described in Autumn et al. (2006a). The RoboToe testing platform consisted of a three-axis piezoelectric force sensor (Kistler, Winterthur, Switzerland) attached to a specialized chuck for SEM specimen stubs. NaOH-cleaned glass slides were rigidly affixed to a frame mounted on two linear actuators (Aerotech, Pittsburgh, PA, USA). Hardware motion was directed, and sensor outputs were monitored with a custom LabVIEW program (National Instruments, Austin, TX, USA; see Gravish et al. 2008). Using the two axes of motion provided by the twin actuation stages, we can simulate a lizard pulling its toe proximally across a substrate using

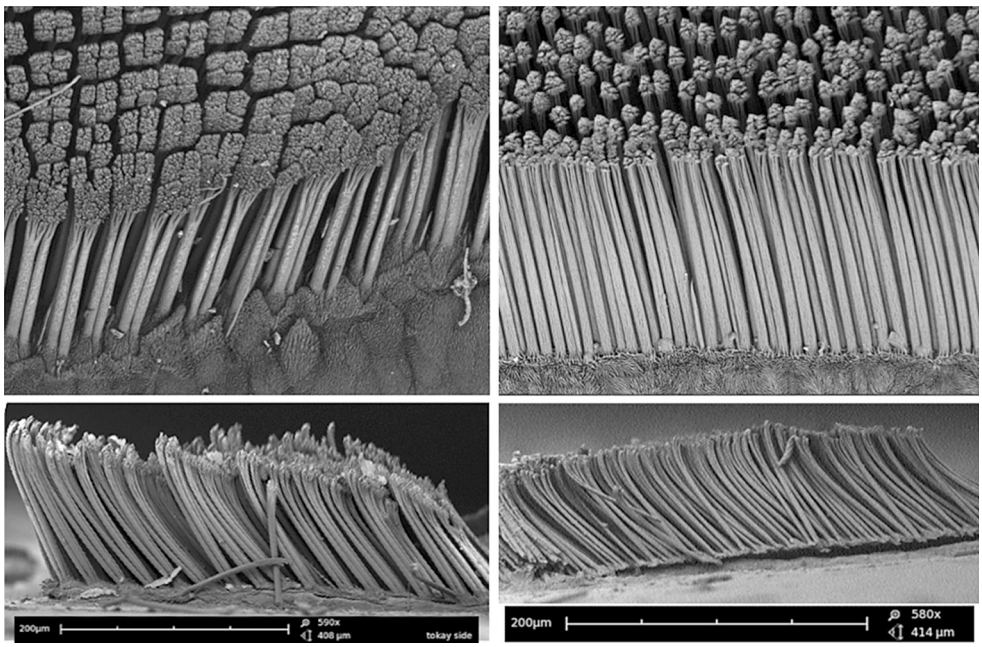

Fig. 4 Setal morphology and organization varied between our two focal species. The *left* images illustrate *G. gecko* setae with *P. grandis* setae displayed in the *right* images. The *top* images display each species pattern of setal organization, with *G. gecko* setae organized in sets of four and unorganized *P. grandis* setae (Peattie Peattie 2007). *Top* images were collected using a FEI NanoSEM 630. The lower images represent typical images collected to quantify setal morphology (see "Material and methods" section)

displacement-controlled motion. We used a camera attached to a long-working-distance microscope (Optem Zoom 100C microscope, Qioptiq, Rochester, NY; DFK 31AF03 CCD camera, Imaging Source, Charlotte, NC) mounted within RoboToe to visualize arrays during testing and measure setal array area (A).

RoboToe can perform multiple automated tests using variable test parameters, such as drag speed and approach distance. All tests were performed at 30 % relative humidity and 25 °C using an environmental enclosure. We recorded frictional and adhesive forces generated by an array during the steady-state "drag" portion of a test at a speed of 0.5 mm/s. By varying the distance between the glass substrate and the base of the array, where it is bonded to a mounting stub, we can identify the optimum working depth of each individual array. A smaller working depth brings the array base closer to the substrate. Optimum depth was defined as the distance in which the highest amount of adhesion was observed. Following the identification of each array's optimum depth, we perform five load-drag-pull (LDP) assays at this depth for each array. A LDP assay allowed an isolated setal array to make contact with a clean glass substrate (load), then moved across the substrate while in contact (drag), and then be removed vertically from contact (pull). From the recorded frictional and adhesive force values, we calculated the critical force angle α* using Eq. (1) for each trial of each array. We used ten isolated setal arrays from four individual live *G. gecko* specimens, and seven arrays isolated from two *P. grandis* individuals for our frictional adhesion measurements.

To measure $\bar{\alpha}^*$, we used 14 live, non-sedated *G. gecko* and five *P. grandis* specimens and an instrumented TAD device similar to that employed by Autumn et al. (2006a). The apparatus consisted of a rotational stage suspended from a force sensor that was controlled and monitored using a custom LabVIEW program. Lizards were suspended from a cleaned glass microscope slide by a single rear center toe. The glass slide was mounted rigidly to the rotational stage and rotated at 1° per second from vertical toward inverted, until the animal spontaneously detached and dropped onto a cushion, an event that was detected by the force sensor. The angle of the glass slide at detachment, relative to vertical, was recorded as an individual toe detachment trial ($\bar{\alpha}$). Multiple TAD trials were conducted with each individual, with a minimum of five trials per individual.

To analyze a dataset of toe detachment measurements, we used the Weibull distribution (Fig. 1a inset (iii)). The Weibull distribution is a continuous probability distribution commonly used to conduct failure analyses (McCool 2012; Pugno and Lepore 2008b; Yang and Xie 2003). The two-parameter Weibull distribution, $p(\bar{\alpha};\ m,\ \lambda)$, provides a failure rate that is proportional to the angle of detachment raised to a power. This is in contrast to the exponential distribution, the expected distribution of waiting times when the failure rate is equal at all times. Using the Weibull probability distribution function, the probability of failure is described as

$$P(\bar{\alpha};\ m, \lambda) = \frac{m(\bar{\alpha})m^{-1}}{\lambda} e^{\left(\frac{\bar{\alpha}}{\lambda}\right)}, \tag{7}$$

where λ is the scale parameter relating to the mean value, and m is a power-law exponent for the distribution (called the "shape parameter," also known as the Weibull

modulus). The mean of the distribution can be calculated as:

$$\bar{\alpha}^* = \lambda\Gamma\left(1+\frac{1}{m}\right) \quad (8)$$

where Γ is the gamma function. We fit each individual lizard's set of observed detachment angles ($\bar{\alpha}$) to a Weibull distribution using maximum likelihood to estimate the mean distribution value for each individual lizard. To estimate a species' mean detachment angle ($\bar{\alpha}^*$) with standard deviations, we calculated the mean and standard deviation of all the species' individual distribution means. We also constructed Quantile–Quantile (Q–Q) plots to investigate the fit of our data to the Weibull distribution.

Work of detachment measurements

To directly measure WoD versus pull-off angle, we used the RoboToe testing platform, and the same isolated setal arrays as our FA assay. We used a similar testing procedure as the FA assay (LDP), but with different pull-off angles θ: 30°, 60°, 90°, 120°, and 150° (during our FA assays, arrays were removed vertically, i.e., 90° from the substrate). Angles under 90° detach in the same direction as the drag phase of testing (proximal with respect to the original orientation of the arrays on the animal before removal). An angle of 90° indicates removal of the array perpendicular to the substrate. Tests with pull-off angles >90° produce retrograde displacement relative to the drag direction, simulating a gecko moving its toe distally while removing it from a substrate (see Fig. 1b). Using the RoboToe testing platform, we are able to produce force–position curves in both the normal and lateral directions. To calculate the work, i.e., energy lost (positive work) or energy recovered (negative work) by the system during each trial in both the normal and lateral directions, we numerically integrated under these curves. We conducted three trials at each angle for each of our 17 isolated setal arrays for a total of 225 trials.

To calculate the expected amount of lateral work ($W_{\parallel\ \mathrm{slip}}$) required to detach setal arrays from a substrate across a set of pull-off angles (θ), we used Eq. (2), our observed mean frictional stress values ($F_{\parallel}$/area) and toe detachment angles ($\bar{\alpha}^*$; see "Introduction" section and Table 4). To calculate $W_{\parallel\ \mathrm{elastic}}$, we followed Gravish et al. (2008) and Persson (2003) using the value 10 in Eq. (3) for the geometrical factor C. We also used a setal lateral displacement distance (x) of 10 and 8 μm for *G. gecko* and *P. grandis*, respectively, which is approximately 10 % of setal length (Gravish et al. 2008), and our observed E_{eff} setal measurements.

Effective modulus measurements

We gathered effective modulus measurements on the same 17 isolated arrays that were used for our FA and WoD tests. Our effective modulus experiments require a different testing routine than our other assays. Since we are only interested in the properties of the array under normal compression, the arrays were brought into contact with cleaned polytetrafluoroethylene-coated glass slides, compressed to their optimum working depth, and then retracted, all along the normal axis. We recorded the normal force generated by each array through a cycle of five vertical compressions (see Fig. 1c for typical results).

Within each resulting force–displacement curve, we identified the beginning and end of the initial elastic loading zone. Elastic loading started when the array came into contact with the substrate, indicated by a significant deviation from zero in observed normal force, taking into account sensor noise. Without a lateral drag, setal crowding can occur before the array's optimum depth is reached during vertical compression. As a result, we assumed the elastic zone ended at a depth of 60 % of an arrays working depth (Pesika et al. 2009; Fig. 1c). We fit a straight line to the elastic loading zone of the force–displacement curve. The slope of this line is the spring coefficient for the array. We performed additional analyses on our force curves, fitting an exponential curve to investigate the shape of the force curves.

We calculated the array effective modulus by multiplying our estimated spring coefficient by the observed array height (for a more detailed description see Autumn et al. 2006b). These constants are then employed in the calculation of E_{eff}. It is important to note that in these calculations, the final values are normalized for array area, by dividing each array's performance by it's area, so E_{eff} is an intrinsic property of the setal array.

Analyses

To estimate species means and standard errors from our observed performance assays (FA, WoD, and EM), we calculated individual mean performance values and averaged these values together. To determine mean species setal morphological measurements, we pooled our observed setal measurements within each species. To compare performance observations between species, we used nested linear mixed-effects models, taking into account within-individual and within-array variation.

Table 1 These variables and constants were used throughout our analyses

Phenotypic variables	
L	Setal length
R	Setal radius
Φ	Setal resting angle
H	Array height
A	Setal array area
ρ	Setal density (Peattie 2007)
d	Array working depth
E	Young's modulus of β-keratin (Autumn et al. 2006b; Gravish et al. 2008)
Frictional adhesion model (*Autumn et al.* 2006a)	
F_{ll}	Frictional force generated by isolated setal arrays in the shear direction
$F_{\perp}$	Adhesive or negative normal force generated by isolated setal arrays
α*	Critical force angle in which setae spontaneously detach with $\alpha^* \geq \tan^{-1}(F_{\perp}/F_{\parallel})$
$\bar{\alpha}^*$	Species-specific toe detachment angle
$\bar{\alpha}$	A single toe detachment angle observation
λ	Weibull scale parameter
m	Weibull shape parameter or modulus
Γ	Gamma function
Work of detachment model (*Gravish et al.* 2008)	
θ	Array pull-off angle
$W_{\text{ll slip}}$	Work of detachment in shear direction due to spatulae slippage
α_0	Angle of setal shaft when under drag tension
$s_{\text{slip }(\theta)}$	Lateral spatulae slip distance for a given pull-off angle of θ
$W_{\text{ll elastic}}$	Elastic energy recovered in the shear direction
k	Estimated setal array lateral spring constant
C	Curvature constant (Persson 2003)
$W_{\perp\text{elastic}}$	elastic energy recovered in the normal direction
x	Recoverable lateral array extension
Effective modulus model (Autumn et al. 2006b*)*	
E_{eff}	Setal array effective elastic modulus
I	Second moment of area for setal fibers treated as cylinders

Using our observed setal morphology means, we used the above biomechanical models to calculate expected performance values. We used setal density values of 14,400 and 28,000 setae/mm^2 for *G. gecko* and *P. grandis* (Peattie 2007), respectively. In previous articles, different values of Young's modulus for β-keratin have been used, with 1.4 GPa in Gravish et al. (2008) and 3.0 GPa in Autumn et al. (2006b). We estimated our expected performance values using both values when appropriate to get a range of expected values. Statistical analyses were conduced in both R statistical software version 2.12.2 (R Core Development Team 2010) and Mathematica version 8.0 (Wolfram Research, Champaign, IL, USA) (see Table 1 for a list of variables used through this study).

Table 2 All errors are reported as standard deviations

Morphological results	*Gekko gecko*	*Phelsuma grandis*
Mean setal length (L)	108 ± 8 m	95 ± 6 μm
Mean setal radius (R)	2.1 ± 0.3 m	1.6 ± 0.1 μm
Mean resting setal shaft angle (ϕ)	48 ± 2°	42 ± 3°
Mean array height (H)	79 ± 7 m	65 ± 4 μm
Mean array area (A)	0.6 ± 0.3 mm^2	0.4 ± 0.1 mm^2
Mean array working depth (d)	39 ± 6 μm	26 ± 3 μm

Morphological measurements were collected from SEM images and RoboToe observations

Results

Morphological comparisons

Both *G. gecko* and *P. grandis* have branched setae with undivided sub-digital scansors, but setal organization differs between the species (Fig. 4). *G. gecko* setae are arranged into sets of four, where as *P. grandis* have unorganized setae (see Fig. 4 and Peattie 2007). The setae of *G. gecko* and *P. grandis* are qualitatively very similar, yet we found significant differences in all observed setal measurements (see Table 2; setal length $F_{1,105} = 88.4$, $p < 0.001$; base to tip $F_{1,107} = 78.0$, $p < 0.001$; radius $F_{1,132} = 170.0$, $p < 0.001$; resting angle $F_{1,55} = 63.4$, $p < 0.001$; array height $F_{1,42} = 53.3$, $p < 0.001$). We suspect these morphological differences, specifically setal length and array height, are responsible for the observed difference in optimum array testing depth (d) between species (see Table 2).

Frictional adhesion measurements

Our experimental results, displayed in Table 3, suggest that the frictional adhesion model effectively describes the performance we observed for both *G. gecko* and *P. grandis* arrays, with friction and adhesion exhibiting a coupled relationship. Figure 5 displays mean array force measurements as stress after being normalized for array area for *G. gecko* (a) and *P. grandis* (b). We calculated adhesion-to-friction force ratios ($F_{\perp}/F_{\parallel}$) using the middle steady-state portion of the observed force-time data. Isolated setal arrays from *P. grandis* exhibited significantly lower mean force ratios than those from *G. gecko* (see Table 3; $t_4 = 3.53$, $p = 0.02$). Using the FA model, we translated these observed setal array force ratios into α* (see "Introduction" and Table 3) to make comparisons to our observed toe detachment and setal shaft angles.

To assess the fit of our toe detachment data to the Weibull distribution, we generated Q–Q plots and found

Table 3 All errors are reported as standard deviations

Performance results	*Gekko gecko*	*Phelsuma grandis*
Frictional adhesion		
Mean observed adhesive stress ($F_{\parallel}/A$)	−90 ± 50 kPa	−110 ± 60 kPa
Extreme observed adhesive stress ($F_{\parallel}/A$)	−266.8 kPa	−295.2 kPa
Mean observed fricitonal stress ($F_{\parallel}/A$)	400 ± 300 kPa	300 ± 100 kPa
Mean observed force ratio ($F_{\parallel}/F_{\parallel}$)	−0.22 ± 0.05	−0.38 ± 0.04
Extreme observed force angles (α*)	24.9°	32.6°
Toe detachment estimate ($\bar{\alpha}^*$)	26 ± 2°	33 ± 1°
Weibull scale parameter (λ)	27 ± 2	34 ± 1
Weibull modulus (m)	14 ± 6	39 ± 27
Work of detachment		
Observed lateral work per area		
Pull angle (θ) of 30°	12 ± 8 J/m^2	7 ± 4 J/m^2
Pull angle (θ) of 60°	5 ± 3 J/m^2	3 ± 1 J/m^2
Pull angle (θ) of 90°	−0.04 ± 0.02 J/m^2	−0.014 ± 0.002 J/m^2
Pull angle (θ) of 120°	−0.7 ± 0.5 J/m^2	−0.5 ± 0.2 J/m^2
Pull angle (θ) of 150°	1.4 ± 0.7 J/m^2	1.6 ± 0.3 J/m^2
Observed normal work per area ($\theta = 120°$)	−0.3 ± 0.4 J/m^2	0.0 ± 0.1 J/m^2
Effective modulus		
Observed setal array elastic modulus (E_{eff})	200 ± 90 kPa	200 ± 80 kPa

These measurements were gathered from RoboToe and toe detachment assays

that our toe detachment observations do match values expected from the Weibull distribution (Fig. 6). After fitting each species toe detachment observations to a Weibull distribution and calculating the distribution mean ($\bar{\alpha}^*$), we found *P. grandis* to have a significantly higher mean toe detachment angle than *G. gecko* ($t_{9.5} = -10.1$, $p < 0.001$). We also compared our observed α* values (calculated from $-\arctan\left[F_{\perp}/F_{\parallel}\right]$) to our observed toe detachment ($\bar{\alpha}^*$) species means. We found our α* values to all be less than our $\bar{\alpha}^*$ values (see Fig. 7), demonstrating that the toe detachment assay is a good predictor of a species' maximum force ratio, as required by the FA model by the use of the inequality in the equation. When we consider our largest observed α* values (see Table 3 and Fig. 7), they are only slightly less then our $\bar{\alpha}^*$ values, suggesting some of our isolated setal arrays were functioning near the upper limit of their performance capabilities.

Work of detachment measurements

Our observed lateral work of detachment measurements (colored dotted lines) are shown alongside our predicted values ($W_{\parallel\ \text{slip}}$, black solid lines) in Fig. 8 and Tables 3, 4. We experimentally observed similar patterns of detachment work across pull-off angles for *G. gecko* (a) and *P. grandis* (b). For both species, normalized work decreased to zero or below over pull-off angles from $\theta = 30°$ to 120°, then increased, suggesting similar overall micromechanics during detachment. To statistically compare our experimentally observed results between species, we used a linear model, testing for the effect of pull-off angle, species, and the interaction term between species and pull-off angle (excluding the measurements at $\theta = 150°$ because the amount of work required for detachment rises with pull-off angles above 120°). When we considered the total work required, with the total work combining lateral and normal components, we found the pull-off angle ($p < 0.001$) and species by pull-off angle interaction ($p = 0.04$) terms were significant; suggesting that the slope of the total work curve across pull-off angles differs between species. When the same linear model was used considering only the lateral work component, pull-off angle was still significant ($p < 0.001$) while the interaction term was not ($p = 0.06$). We also used a linear model to compare our expected lateral work between species using the terms species, pull-off angle and the interaction term between species and pull-off angle (excluding $\theta = 150°$). In this comparison, the interaction term was significant ($p = 0.009$), similar to analyses from our observed work (see above).

When we consider the similarity between our predicted and observed lateral work values (Fig. 8), we found our models accurately predicted the shape of the curve, with work decreasing toward pull-off angles of 120°. We predicted less lateral work at higher pull-off angles for *G. gecko* (Fig. 8a), although our predicted work values are all within two standard deviations of our observed values except for when θ was 90°. Our observed and predicted lateral work for *P. grandis* also appear similar (Fig. 8b), but our predicted values were over two standard deviations above from our observed values for $\theta = 90°$, 120°, and 150°.

We also estimated the returned elastic energy per area stored in the setae during detachment paths with little to no spatulae slippage ($W_{\parallel\ \text{elastic}}$ and $W_{\perp\text{elastic}}$) and compared these values to our lateral and normal observed work measurements at $\theta = 120°$ (see Eqs. 3, 4, and 5, Tables 3, 4). Due to the returned energy stored in the setae and very little spatulae slippage, we expect the work of detachment at a pull-off angle of 120° to be negative. We found our expected lateral energy return values, which considered multiple values for Young's modulus of β-keratin, to be within two standard deviations of our observed values for both focal species. However, our expected normal energy return values were over two standard deviations less than our observed measurements for both species.

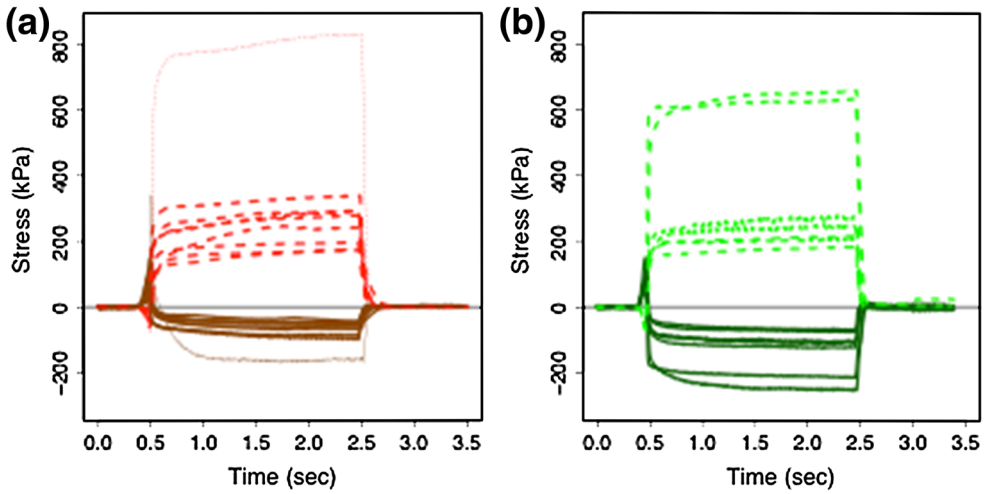

Fig. 5 We directly observed frictional and adhesive stress generated over time of each isolated setal array for *Gekko gecko* (plot **a**, *red dashed lines* are frictional stress, *brown solid lines* are adhesive stress) and *Phelsuma grandis* (plot **b**, *green dashed lines* are frictional stress, *dark green solid lines* are adhesive stress). In this figure, the five LDP trials of each array were averaged for each time point. Stresses were calculated by dividing the mean observed forces by array area, allowing for within and between species comparisons. Note that stress on the *y-axis* ranges from −200 to 800 kPa for both plots to allow the performance variation between arrays to be seen. There is one *G. gecko* and two *P. grandis* arrays that generated substantially more stress than the others. This is due to their smaller size, roughly half as large as the others. When using smaller arrays, a larger proportion of setae are able to make appropriate contact with the substrate, with fewer setae over-compressed into the substrate. As a result, when adjusted for area, smaller arrays generate higher stress

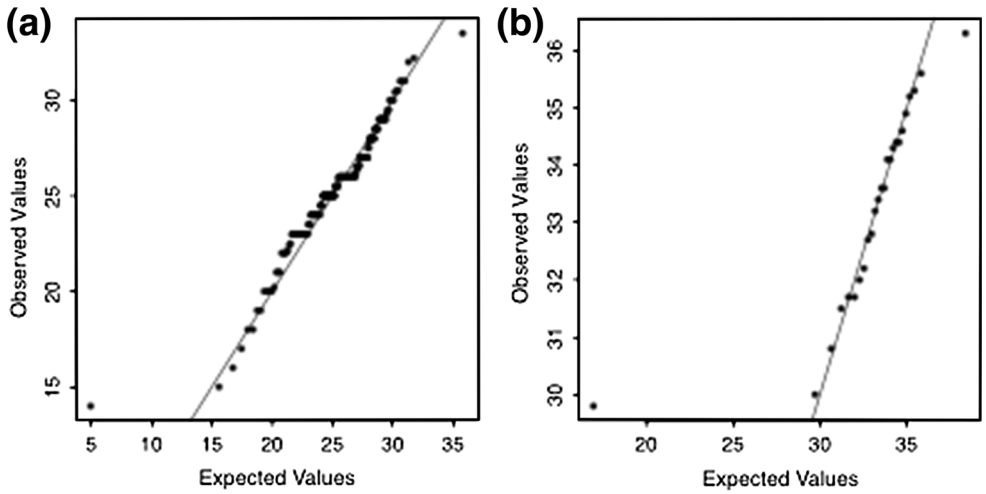

Fig. 6 To evaluate the fit of our toe detachment observations ($\bar{\alpha}^*$) to the Weibull distribution, we constructed Q–Q plots. In these plots, expected values from the Weibull distribution ($m = 10$ and $\lambda = 26$ and 33 for *G. gecko* **a** and *P. grandis* **b**, respectively) are plotted against observed values. If the Weibull distribution is a good fit to our data, the resulting points should lie on a line through the origin with slope of 1. Based on our plots, we can conclude that our data fits the Weibull distribution well. The datasets from both our focal species display extreme points that do not lie on this line. These points suggest that, rarely, the Weibull distribution would contain additional values that are larger and smaller than our observed values (We simulated 10,000,000 using the Weibull distribution to construct these plots)

Effective modulus measurements

The isolated setal arrays of both focal species behaved as linear springs (initially) when compressed in the normal direction, producing similar effective modulus values for both species. Different regimes of stiffness, corresponding to different degrees of crowding among the setae could be seen in our results. To evaluate the presence of discrete phases of contact, we fitted a two-segmented line to our force–displacement curves. If distinct phases of compression were present, i.e., elastic compression switching to setal crowding, where the setae begin to contact each other, a two-segmented line should fit our data well. We also fit an exponential

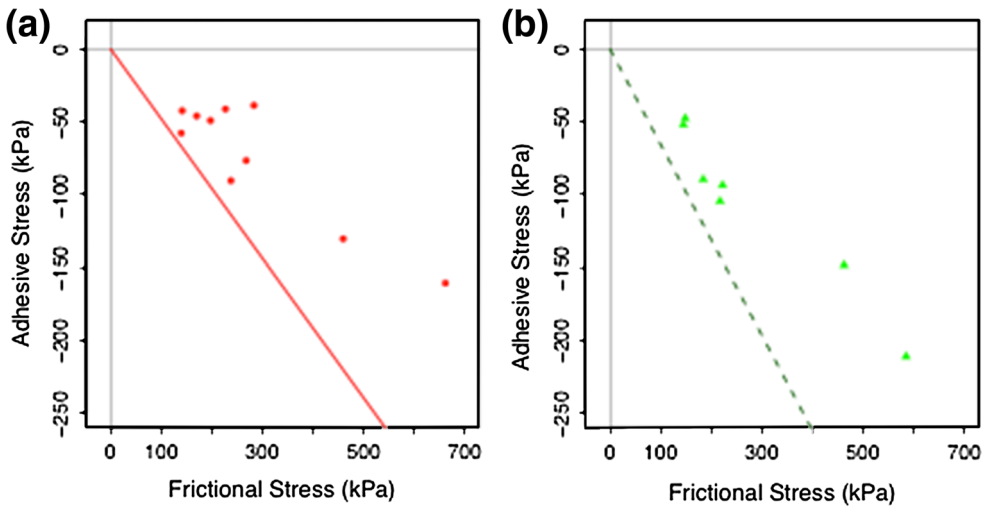

Fig. 7 We directly observed the mean frictional and adhesive stresses generated by each isolated setal array for *G. gecko* (plot **a**, *red dots*) and *P. grandis* (plot **b**, *green triangles*). Stresses were calculated by averaging the observed forces divided by array area from each array's set of five LDP trials. Note that the *y-axis* and *x-axis* are equivalent in both plots to allow the performance variation between arrays to be seen. Our observed toe detachment species means ($\bar{\alpha}^*$), are plotted as the limiting force angle indicated as a line with slope equal to tan ($\bar{\alpha}^*$), illustrated as a red, solid line in the *G. gecko* plot and a *dark green dashed line* in the *P. grandis* plot. All of our observed setal force ratios fall to the right of the limiting values established by the TAD measurements, suggesting toe detachment is a good predictor of a species maximum force ratio

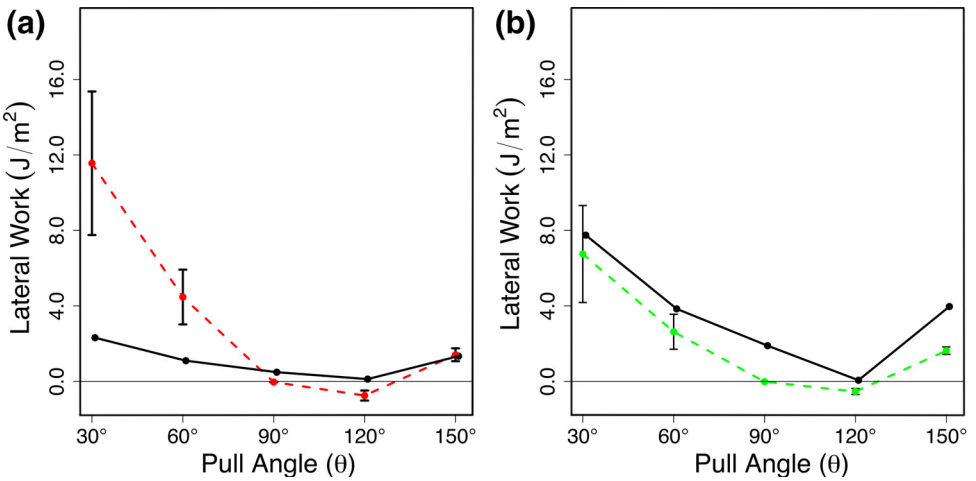

Fig. 8 We directly observed the lateral work per area associated with setal array detachment across a set of detachment angles for *G. gecko* (*red dashed line*, plot **a**) and *P. grandis* (*green dashed line*, plot **b**). It can be seen that work per area decreases as pull-off angle approaches 120°. Additionally, we estimated lateral work per area using setal morphology ($W_{\| \text{ slip}}$, *solid black lines*). Notice in both graphs, the *y-axis* (normalized lateral work) ranges from 0 to 16 J/m^2. Our predictions of lateral work per area do exhibit a similar pattern across pull-off angles, with decreasing work in pull-off angles from 30° to 120°, but with species-specific inaccuracies (see Results and Discussion section)

curve to our force–displacement measurements. We found some trials did fit the expected pattern with distinct zones of contact, while other trials were very curve-like. There was also a species effect, with *G. gecko* trials more often curve-like then *P. grandis*, suggesting complex interactions between setae during compression. When comparing our expected isolated setal array effective modulus, calculated using a range of values for the Young's modulus of β-keratin, to our observed values, we found the entire range of our modulus estimates (Table 4) to be within two standard deviations of our observations for both focal species.

Table 4 We predicted setal performance and compared these values to observed performance using our morphological measurements as input values into our WoD and EM mathematical models

Model results	Predicted *G. gecko*	Observed *G. gecko*	Predicted *P. grandis*	Observed *P. grandis*
Work of detachment				
Setal shaft angle under tension (α_0)	24.0°	–	25.2°	–
Shear work per area ($W_{\parallel\ slip}$)				
Pull angle (θ) of 30°	2.3 J/m^2	12 ± 8 J/m^2	7.8 J/m^2	7 ± 4 J/m^2
Pull angle (θ) of 60°	1.1 J/m^2	5 ± 3 J/m^2	3.8 J/m^2	3 ± 1 J/m^2
Pull angle (θ) of 90°	0.49 J/m^2	−0.04 ± 0.02 J/m^2	1.9 J/m^2	−0.014 ± 0.002 J/m^2
Pull angle (θ) of 120°	0.12 J/m^2	−0.7 ± 0.5 J/m^2	0.061 J/m^2	−0.5 ± 0.2 J/m^2
Pull angle (θ) of 150°	1.3 J/m^2	1.4 ± 0.7 J/m^2	4.0 J/m^2	1.6 ± 0.3 J/m^2
Setal array lateral spring constant (k)	0.21–0.45 N/m	–	0.11–0.24 N/m	–
Shear elastic return ($W_{\parallel\ elastic}$)	−0.15 to −0.32 J/m^2	−0.7 ± 0.5 J/m^2	−0.10–0.21 J/m^2	−0.5 ± 0.2 J/m^2
Normal elastic return ($W_{\perp\ elastic}$)	−2.4 J/m^2	−0.3 ± 0.4 J/m2	−2.1 J/m^2	0.0 ± 0.1 J/m^2
Effective modulus				
Setal array elastic modulus (E_{eff})	130–270 kPa	200 ± 90 kPa	82–180 kPa	200 ± 80 kPa

When values of Young's modulus of β-keratin (E) were needed, we evaluated the models using both 1.4 GPa and 3.0 GPa to get a range of possible performance values

Discussion

Model accuracy

We tested the validity of established gecko performance models using empirical and predicted performance values of isolated setal arrays from one previously considered gecko species and one novel species. We found that these models did succeed in predicting many aspects of array performance, but also indicated some interesting differences from our observed values. When considering our results for *G. gecko*, we observed similar performance values as previously published studies in which our focal models were originally described, suggesting that our isolated arrays were functional and not damaged.

We found the FA model accurately described the relationship between setal critical angle, friction, and adhesion generated for both focal species. Our WoD model calculations reproduced the form of the $W_{\parallel\ slip}(\theta)$ curves (Eq. 2, Fig. 8), but there were significant quantitative differences. In our calculations of $W_{\parallel\ slip}$, we used our toe detachment estimates, $\bar{\alpha}^*$, as the critical detachment values. In Autumn et al. (2006a), the authors observed that setal detachment angle (α*) differed from the observed toe detachment angle ($\bar{\alpha}^*$). Setal detachment angle (α*) was reported as 30° for *G. gecko*, approximately 120 % of toe detachment angle (Autumn et al. 2006a). Using this factor, we also estimated *P. grandis* setal detachment angle and reevaluated Eq. 2 using setal detachment angle (α*) in place of $\bar{\alpha}^*$ for both focal species. These alternative $W_{\parallel\ slip}$ values still displayed idiosyncratic inaccuracies, with estimates at low angles more accurate for *G. gecko*, but less accurate at higher pull-off angles. Estimates for *P. grandis* were less accurate and higher then previous predictions across all pull-off angles.

When considering the EM model, we were able to accurately predict the observed effective modulus of isolated setal arrays for both *G. gecko* and *P. grandis* (Eq. 6), but our results also suggest that setal arrays may not always exhibit clearly delineated phases of compression, occasionally displaying nonlinear force–displacement curves. This result suggests setal crowding may be a complex process (Pesika et al. 2009), possibly influenced by setal organization, morphology, and the condition of the specimen. Using a model incorporating nonlinear stiffness, with the effective modulus also dependent on compression depth, may more accurately predict array performance.

The previously published mathematical models considered in this study (Autumn et al. 2006a, 2006b; Gravish et al. 2008) were validated by our results, highlighting their utility as general principles of how geckos' complex adhesive system functions. These models are templates—the simplest model that explains general system function (Full and Koditschek 1999). Our results also suggest that models more fully anchored in the morphology of the animal will be required to study the variation among and within species (Full and Koditschek 1999). Previous work has illustrated substantial setal variation within an individual gecko's toe pad, as well as between species. Setal length in *G. gecko* ranges from under 5 μm to over 100 μm (Johnson and Russell 2009; Russell 1979). Additional model complexity, such as drawing from distributions of setal lengths in place of point estimates to predict a distribution of possible performance values or incorporating scansor shape, will help to elucidate the effect

morphological variation across the toe pad may have on performance. With this approach, we can move toward a better understanding of the evolutionary processes that led to the origination and refinement of this novel biological adhesive system.

Species comparisons and ecology

Our study found many interesting similarities and differences between our focal species. Both of our focal species have undivided scansors, with *G. gecko* also possessing claws, whereas functional claws have been lost in the *Phelsuma* genus (Russell 1977). Overall, our results suggest similar setal mechanics for both species regarding the production of adhesion, energy storage during setal attachment, and the effective stiffness of setal arrays. While we found support for similar processes that may represent a common theme for how all gecko setae operate, we did find performance differences between our species that suggest small morphological differences likely have large effects on performance. Our observed differences in adhesive performance cannot be explained simply by a difference in setal shaft angle under tension, α_0, as might have been expected. Other setal morphological characters likely contribute to variation in $\bar{\alpha}^*$ between species, such as the miter angle, which measures how the spatulae are aligned in space at the tip of the setae (Fig. 2).

Our results also pose the question of how the gecko adhesive system may be adapted to particular microhabitats. Hecht (1952) found selection for more lamellae in large *Aristelliger praesignis* geckos. Generating larger amounts of adhesion may be beneficial on highly inverted perches, where a large part of the animal's body weight needs to be supported by the adhesive system, or on rough perches where only a small amount of surface area is available for contact (Huber et al. 2007; Pugno and Lepore 2008a; Russell and Johnson 2007). Another consideration is that large adhesive forces may not always be beneficial. There is a potential trade-off regarding the production of adhesion and friction. Species with high detachment angles may have setae and spatulae that perform best with large setal shaft angles, producing both friction and adhesion, but less absolute friction than if the setal shaft angle was smaller. In this scenario, a species with a high detachment angle may sacrifice the amount of absolute friction generated for a combination of adhesion and friction.

Studies of *Anolis* lizards, a well-studied group of non-gecko lizards with convergent adhesive toe pads (Losos 2009), have found that species with more lamellae or larger pads use perches higher in the canopy (Elstrott and Irschick 2004; Glossip and Losos 1997; Irschick et al. 2006). *Anolis* lizards have short setae, ranging from 15 to 30 μm, and generate low levels of adhesion with detachment angles from 15° to 20° (Hagey 2013; Ruibal and Ernst 1965). They are also very rarely, if ever, observed on fully inverted perches (J. Losos and R. Glor, personal communication). We may use this insight to make habitat use predictions for gecko species with similar morphology and performance. For example, *Rhacodactylus ciliatus*, an arboreal gecko species found in New Caledonia, have short setae (47 μm long; Peattie 2007) and exhibit a low detachment angle of 19° (Hagey 2013). Based on this information, we may predict *R. ciliatus* typically occupy vertical perches similar to *Anolis* lizards, a prediction supported by observations of *R. ciliatus* in captivity (TH, pers. obs.).

When we consider our WoD results, we again find evidence of a common mechanism of energy storage for gecko species with similar setae, but with species-specific differences. *P. grandis* was found to store less energy during attachment. This difference may affect how our focal species move and detach their feet and toes during locomotion in the wild. Perch angle is known to effect foot orientation (Russell and Higham 2009), and hence, perches with different orientations may require different strategies while also maintaining stability, such as the use of digit hyperextension or distal movement of the toe. Work of detachment may have a complex interaction with gecko walking and running kinematics on horizontal, vertical, and fully inverted surfaces (Spezzano and Jayne 2004).

Lastly, the effective moduli of our focal species were similar, but this may not be true for all geckos. For example, *R. ciliatus* have a relatively low setal aspect ratio of 0.032, with a setal diameter of 1.5 μm and length of 47 μm, as compared with *Thecadactylus rapicauda*, an arboreal species from South America, with an aspect ratio of 0.064 due to setae 6.0 μm in diameter and 94 μm in length (Peattie 2007). Considering only aspect ratio, we may predict *R. ciliatus* to have a lower effective modulus as compared with *T. rapicauda*.

Natural surfaces are rarely perfectly flat, such as tree bark or rocks. Intimate contact between a gecko's adhesive system and their substrate is required for such attachment, and the effective modulus of setae may dictate this interaction. Softer arrays may contact more surface area on rough surfaces with highly variable topology, while stiffer arrays may store more energy under tension, allowing for more friction and stronger attachment on smoother surfaces. If an environment requires setae to be highly compliant, i.e., favoring a low effective modulus such as is found in species with low setal density or aspect ratio, there may exist a trade-off between compliance and attachment strength, suggesting different morphologies and capabilities will be beneficial in different environments.

The ability to move through an environment quickly and consistently is immensely valuable for geckos in the wild,

requiring a finely tuned adhesive system that balances adhesion and friction generation, detachment and compliance requirements on a wide variety of surface topologies. Few studies have considered habitat use of geckos in the wild (but see Russell and Johnson 2007), yet there are over 1,400 described gecko species from over 100 genera (Gamble et al. 2012). Across these species, there is a wide variety of gross and microscopic morphological variation in the adhesive system (Gamble et al. 2012; Johnson and Russell 2009; Russell 1979), suggesting variation in performance capabilities may be important for how different species of geckos navigate their environments. Ecological observations of geckos with various setal morphologies in natural settings will allow a stronger understanding of the evolutionary and ecological pressures present on the gecko adhesive system, specifically describing how particular morphologies and capabilities are linked to different microhabitats. Evaluating how different toe pad and setal morphologies influence adhesive performance can help us understand how geckos have adapted to different habitats.

Acknowledgments We thank four previous anonymous reviewers, Craig McGowan, Mitch Day, Chloe Stenkamp-Strahm, the Harmon, Rosenblum, and Autumn labs for helpful advice and comments, Matt Wilkinson for assistance with laboratory equipment, Katie Pond and Christine Van Tubbe for help with animal care, Meghan Wagner and Andrew Schnell for assistance in the laboratory, and the University of Idaho IACUC for approval of the project (Protocol #2010-40). Aaron Bauer and Todd Jackman also provided assistance and support. We thank the University of Idaho and the National Science Foundation (DEB-0844523, IOS-0847953 and NBM-0900723) for funding.

References

Alibardi L, Toni M, Dalla Valle L (2007) Expression of beta-keratin mRNAs and proline uptake in epidermal cells of growing scales and pad lamellae of gecko lizards. J Anat 211(1):104–116

Autumn K, Liang YA, Hsieh ST, Zesch W, Chan WP, Kenny TW, Fearing R, Full RJ (2000) Adhesive force of a single gecko foothair. Nature 405(6787):681–685

Autumn K, Sitti M, Liang YA, Peattie AM, Hansen WR, Sponberg S, Kenny TW, Fearing R, Isrealachvili JN, Full RJ (2002) Evidence for van der Waals adhesion in gecko setae. Proc Natl Acad Sci USA 99(19):12252–12256

Autumn K, Dittmore A, Santos D, Spenko M, Cutkosky M (2006a) Frictional adhesion: a new angle on gecko attachment. J Exp Biol 209(18):3569–3579

Autumn K, Majidi C, Groff RE, Dittmore A, Fearing R (2006b) Effective elastic modulus of isolated gecko setal arrays. J Exp Biol 209(18):3558–3568

Bauer AM (1998) Morphology of the adhesive tail tips of carphodactyline geckos (Reptilia: Diplodactylidae). J Morphol 235 (1):41–58

Chen B, Wu PD, Gao H (2008) Hierarchical modelling of attachment and detachment mechanisms of gecko toe adhesion. Proc R Soc A 464(2094):1639–1652

Chen B, Wu P, Gao H (2009) Pre-tension generates strongly reversible adhesion of a spatula pad on substrate. J R Soc Interface 6(35):529–537

Elstrott J, Irschick DJ (2004) Evolutionary correlations among morphology, habitat use and clinging performance in Caribbean Anolis lizards. Biol J Linn Soc 83(3):389–398

Federle W (2006) Why are so many adhesive pads hairy? J Exp Biol 209(14):2611–2621

Full RJ, Koditschek DE (1999) Templates and anchors: neuromechanical hypotheses of legged locomotion on land. J Exp Biol 202(23):3325–3332

Gamble T, Greenbaum E, Jackman TR, Russell AP, Bauer AM (2012) Repeated origin and loss of adhesive toepads in geckos. PLoS ONE 7(6):e39429. doi:10.1371/journal.pone.0039429

Glaw F, Vences M (2007) A field guide to the amphibians and reptiles of Madagascar. 3rd edn. Köln, Vences & Glaw, Köln, Germany

Glossip D, Losos JB (1997) Ecological correlates of number of subdigital lamellae in anoles. Herpetologica 53(2):192–199

Gravish N, Wilikinson M, Autumn K (2008) Frictional and elastic energy in gecko adhesive detachment. J R Soc Interface 5 (20):339–348

Hagey TJ (2013) Mechanics, diversity, and ecology of Gecko adhesion. University of Idaho, Moscow

Hansen WR, Autumn K (2005) Evidence for self-cleaning in gecko setae. Proc Natl Acad Sci USA 102(2):385–389

Hecht MK (1952) Natural selection in the lizard genus *Aristelliger*. Evolution 6(1):112–124

Huber G, Gorb SN, Hosoda N, Spolenak R, Arzt E (2007) Influence of surface roughness on gecko adhesion. Acta Biomater 3 (4):607–610

Irschick DJ, Austin CC, Petren K, Fisher RN, Losos JB, Ellers O (1996) A comparative analysis of clinging ability among pad-bearing lizards. Biol J Linn Soc 59(1):21–35

Irschick DJ, Herrel A, Vanhooydonck B (2006) Whole-organism studies of adhesion in pad-bearing lizards: creative evolutionary solutions to functional problems. J Comp Physiol A 192 (11):1169–1177

Johnson MK, Russell AP (2009) Configuration of the setal fields of *Rhoptropus* (Gekkota: Gekkonidae): functional, evolutionary, ecological and phylogenetic implications of observed pattern. J Anat 214(6):937–955

Losos JB (2009) Lizards in an evolutionary tree: the ecology of adaptive radiation in anoles. University of California Press, Berkeley

Maderson PFA (1964) Keratinized epidermal derivatives as an aid to climbing in gekkonid lizards. Nature 203(4946):780–781

McCool JI (2012) Using the Weibull distribution: reliability, modeling and inference, vol 950. Wiley, London

Peattie AM (2007) The function and evolution of Gekkotan adhesive feet. Doctor of Philosophy, University of California, Berkeley

Peattie AM (2009) Functional demands of dynamic biological adhesion: an integrative approach. J Comp Physiol B 179(3):231–239

Persson BNJ (2003) On the mechanism of adhesion in biological systems. J Chem Phys 118(16):7614–7621

Pesika NS, Gravish N, Wilkinson M, Zhao B, Zeng H, Tian Y, Israelachvili J, Autumn K (2009) The crowding model as a tool to understand and fabricate gecko-inspired dry adhesives. J Adh 85(8):512–525

Pugno NM, Lepore E (2008a) Observation of optimal gecko's adhesion on nanorough surfaces. BioSystems 94(3):218–222

Pugno NM, Lepore E (2008b) Living Tokay geckos display adhesion times following Weibull statistics. J Adh 84(11):949–962

Puthoff JB, Prowse MS, Wilkinson M, Autumn K (2010) Changes in materials properties explain the effects of humidity on gecko adhesion. J Exp Biol 213(Pt 21):3699–3704

Pyron RA, Burbrink FT, Wiens JJ (2013) A phylogeny and revised classification of Squamata, including 4161 species of lizards and snakes. BMC Evol Biol 13(1):93

Rosler H, Bauer AM, Heinicke MP, Greenbaum E, Jackman T, Nguyen TQ, Ziegler T (2011) Phylogeny, taxonomy, and zoogeography of the genus *Gekko* Laurenti, 1768 with the revalidation of *G. reevesii* Gray, 1831 (Sauria: Gekkonidae). Zootaxa 2989:1–50

Ruibal R, Ernst V (1965) The structure of the digital setae of lizards. J Morphol 117(3):271–293

Russell AP (1977) Genera *Rhoptropus* and *Phelsuma* (Reptilia Gekkonidae) in Southern-Africa—case of convergence and a reconsideration of biogeography of *Phelsuma*. Zool Afr 12 (2):393–408

Russell AP (1979) Parallelism and integrated design in the foot structure of gekkonine and diplodactyline geckos. Copeia 1979 (1):1–21

Russell AP (2002) Integrative functional morphology of the gekkotan adhesive system (Reptilia: Gekkota). Integr Comp Biol 42 (6):1154–1163

Russell AP, Higham TE (2009) A new angle on clinging in geckos: incline, not substrate, triggers the deployment of the adhesive system. Proc R Soc B 276(1673):3705–3709

Russell AP, Johnson MK (2007) Real-world challenges to, and capabilities of, the gekkotan adhesive system: contrasting the rough and the smooth. Can J Zoolog 85(12):1228–1238

Spezzano LC Jr, Jayne BC (2004) The effects of surface diameter and incline on the hindlimb kinematics of an arboreal lizard (*Anolis sagrei*). J Exp Biol 207(Pt 12):2115–2131

Tian Y, Pesika N, Zeng H, Rosenberg K, Zhao B, McGuiggan P, Autmn K, Israelachvili J (2006) Adhesion and friction in gecko toe attachment and detachment. Proc Natl Acad Sci USA 103 (51):19320–19325

Williams EE, Peterson JA (1982) Convergent and alternative designs in the digital adhesive pads of Scincid lizards. Science 215 (4539):1509–1511

Yamaguchi T, Gravish N, Autumn K, Creton C (2009) Microscopic modeling of the dynamics of frictional adhesion in the gecko attachment system. J Phys Chem B 113(12):3622–3628

Yang ZL, Xie M (2003) Efficient estimation of the Weibull shape parameter based on a modified profile likelihood. J Stat Comput Simul 73(2):115–123